Sensors & Actuators: B. Chemical 293 (2019) 166–172

Contents lists available at ScienceDirect

Sensors and Actuators B: Chemical

journal homepage: www.elsevier.com/locate/snb

YSZ-based mixed-potential type highly sensitive acetylene sensor based on porous SnO_2/Zn_2SnO_4 as sensing electrode

Caileng Wang[a], Ao Liu[a], Xueli Yang[a], Jing Wang[a], Rui You[b], Zijie Yang[a], Junming He[a], Lianjing Zhao[a], Fangmeng Liu[a,*], Xu Yan[a], Xishuang Liang[a], Yuan Gao[a], Fengmin Liu[a], Peng Sun[a], Geyu Lu[a,*]

[a] State Key Laboratory on Integrated Optoelectronics, Key Laboratory of Advanced Gas Sensors, College of Electronic Science and Engineering, Jilin University, 2699 Qianjin Street, Changchun, Jilin Province, 130012, China
[b] Department of Precision Instrument, Tsinghua University, Beijing 100084, China

ARTICLE INFO

Keywords:
C_2H_2sensor
Porous SnO_2/Zn2SnO4
YSZ
Mixed-potential

ABSTRACT

Here, the porous SnO_2/Zn_2SnO_4 sensing electrode material prepared by facile hydrothermal method was applied to fabricate the mixed-potential-type gas sensor based on yttrium-stabilized zirconia (8 mol% Y_2O_3-doped ZrO_2) solid electrolyte plane substrate for effectively detecting acetylene (C_2H_2) at 700 °C. In terms of the sensing characteristics of the C_2H_2 gas sensor, the response value toward 100 ppm C_2H_2 was -82.3 mV, and the detection limit of C_2H_2 was lowered to 500 ppb. The ΔV of the sensing device varied piecewise linearly with the logarithm of C_2H_2 concentration gradient range of 0.5–2 and 5–1000 ppm, with sensitivities of -12 and −56 mV/decade, respectively. In addition, the sensor exhibited good humidity stability, long stability, and selectivity to C_2H_2 at 700 °C. More interestingly, after high-temperature measurement (700 °C) for 20 consecutive days, the sensor continued to present good response transients, sensitivity, and reproducibility to C_2H_2. Furthermore, the sensing mechanism of the mixed-potential-type sensor was verified by measuring the polarization curves and complex impedance curves.

1. Introduction

The development of society and demand of human production and lives are inseparable from electricity; the power transformer is a very important power conversion equipment in the entire power system; therefore, its various aspects of hidden dangers and failures must be taken seriously and solved [1–3]. The oil-immersed transformer is mainly used in the industry; it uses an oil-paper insulation structure to prevent insulation safety problems during long-term operation of the transformer. When the transformer generates an electrical fault or a thermal fault, different types of characteristic gases including acetylene (C_2H_2) are produced. In this regard, different fault types, such as spark discharge, arc discharge, and partial discharge, can be judged by detecting acetylene gas around transformers. Furthermore, acetylene is a common flammable and explosive hazardous gas, which causes environmental pollution and dangerous accidents extremely easily once combustion and explosion occur [4–6]. Therefore, real-time, online, and in situ detection of acetylene is of great significance to eliminate the potential risks of transformers and ensure normal operation of equipment and safety of operators.

To achieve accurate detection of acetylene, many methods such as gas chromatography [7], infrared spectroscopy [8], Raman spectroscopy [9], photoacoustic spectroscopy [10], and metal oxide semiconductor sensors [11] have been proposed. However, given the enormous volume and exorbitant price, the methods based on gas chromatography and spectral absorption instruments are usually suitable for laboratory even if they have high precision. For metal oxide semiconductor-type C_2H_2 gas sensor, low sensitivity [12–14] and long response–recovery time remain essential factors that limit the widespread use of such sensors [11,15,16]. Considering these shortcomings, an all-solid mixed-potential-type gas sensor based on oxide sensing electrode (SE) and yttrium-stabilized zirconia (YSZ) solid electrolyte with high C_2H_2 sensing performance needs to be developed. The high sensing property of the mixed-potential-type gas sensor depends on the selection of oxide sensing materials and the electrochemical reaction degree at the three-phase boundary (TPB). To date, different sensing materials, such as single oxide [17,18], perovskite [19,20] and spinel oxides [21,22], and other composite oxides [23,24], have been

* Corresponding authors.
E-mail addresses: liufangmeng@jlu.edu.cn (F. Liu), lugy@jlu.edu.cn (G. Lu).

https://doi.org/10.1016/j.snb.2019.05.006
Received 1 December 2018; Received in revised form 25 April 2019; Accepted 3 May 2019
Available online 06 May 2019
0925-4005/

developed to fabricate a high-performance YSZ-based mixed-potential-type gas sensor for the detection of different gases. Combining SnO_2, which has stable chemical properties, and Zn_2SnO_4, which has high electron mobility and high chemical sensitivity, is believed to show greater gas sensing properties to the target gas [25–32]. Moreover, as reported in previous studies [33], the microstructure and porosity of sensing materials are conducive to improve the sensing characteristics of fabricated sensing devices because of the increase in gas diffusion degree in the SE layer and increase of TPB. Inspired by these research results, we chose to design the SnO_2/Zn_2SnO_4 SE material with a porous structure and fabricate a YSZ-based C_2H_2 gas sensor on the basis of a mixed-potential mechanism.

This study is the first to fabricate a YSZ-based mixed-potential-type C_2H_2 sensor that uses porous SnO_2/Zn_2SnO_4 as the SE. The sensing properties of the fabricated C_2H_2 sensor were measured and investigated in detail. Furthermore, the sensing mechanism of the gas sensor to C_2H_2 was discussed.

2. Experimental

2.1. Synthesis and characterization of the porous SnO_2/Zn_2SnO_4 composite oxide

The porous SnO_2/Zn_2SnO_4 composite oxide SE material was successfully synthesized via the typical hydrothermal method, as reported in literature [34]. The precursor was annealed in a muffle furnace at 800 °C with heating rate of 2 °C/min for 2 h to obtain the porous SnO_2/Zn_2SnO_4 sensing material.

The crystalline structure of the SnO_2/Zn_2SnO_4 sensing material was determined by operating a Rigaku wide-angle X-ray diffractometer (D/max rA) using Cu Kα radiation (λ = 1.5410 Å) in an angle range of 10°–80°. The morphology and grain size were observed using field emission scanning electron microscopy (JEOL JSM-6500 F, accelerating voltage = 15 kV).

2.2. Fabrication and measurement of gas sensor

The manufacturing process of the gas sensor is as follows. First, both sides of a YSZ substrate (8 mol% Y_2O_3-doped, 2 mm × 2 mm square, 0.3 mm thickness, provided by Anpeisheng Corp., China) were used to produce a Pt reference electrode (RE) and point-shaped with Pt wire using commercial Pt paste (Sino-Platinum Metals Co., Ltd.). Second, the SE paste was acquired by mixing the SnO_2/Zn_2SnO_4 sensing material with a few drops of deionized water. Then, the paste was painted on the point-shaped Pt to form a stripe-shaped SE. Next, the device was transferred to a muffle furnace for sintering at 800 °C for 2 h to facilitate improved contact between YSZ and sensing material. Finally, an "m" symbol Pt heater, which could provide the required working temperature to the device on the Al_2O_3 substrate, was integrated into the YSZ plate using an inorganic adhesive to form a complete gas sensor. Fig. 1 shows a schematic illustration of the fabricated gas sensor.

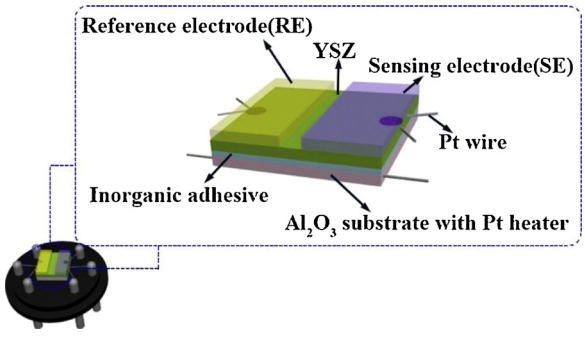

Fig. 1. Schematic illustration of the gas sensing device.

A static test system was used for measuring the gas sensing properties. Approximately 1% of the C_2H_2 standard gas including 1% C_2H_2 and nitrogen equilibrium gas, which is purchased from Changchun Juyang Gas Co., Ltd, was used to gain different concentrations of C_2H_2 test gases by diluting with air in a 1 L measurement chamber. First, the test chamber was pumped into vacuumed and then filled with pure air. Subsequently, a certain amount of C_2H_2 or other gases was mixed into the chamber via a special airlock at the side of the chamber using a microsyringe to distribute the test gases uniformly. A digital electrometer (Rigol DM3054) was used for measuring the electric potential between the SE and RE when the device was placed in the air or in the sample atmosphere. A constant current source (Gwinstek gpd-3303 s) was used to provide a stable heating current to the heater to ensure the heating power of the heating plate. The heating temperature can be adjusted by adjusting the current. The surface temperature of the device can be calibrated by the infrared temperature measuring instrument (Flur T250). For the humidity test of the sensor, we used a constant temperature and humidity chamber (Shanghai ESPC Environment Equipment Corporation, China) to provide a different humidity atmosphere for the 1 L test chamber. The measurement data were recorded in a computer that was linked to the electrometer. The current–voltage (polarization) curves of the device were obtained using two electrodes in air and the target gases through the potentiodynamic method (CHI600C, Instrument Corporation of Shanghai, China). Furthermore, complex impedance results were recorded depending on the impedance analyzer (Solartron 1260 and Solartron 1287) with the amplitude of the AC potential signal at 300 mV and the frequency from 1 MHz to 0.1 Hz at 700 °C.

3. Result and discussion

The crystal phase structure and composition of the sensing material can be analyzed based on the X-ray diffraction (XRD) spectra. Fig. 2(a) shows the XRD pattern of the synthesized porous SnO_2/Zn_2SnO_4 sample. As shown in the figure, the major diffraction peaks of the sensing material were in accordance with the standard diffraction data of SnO_2 (JCPDS# 41–1445) and Zn_2SnO_4 (JCPDS# 24–1470). The well peak intensity and narrow peak width manifested good crystallinity and small particle size of the sensing material. The surface morphology of porous SnO_2/Zn_2SnO_4 composite oxide observed by SEM is shown in Fig. 2(b). The composite oxide was composed of a uniformly distributed sphere-shaped particle with a diameter of approximately 480 nm. Furthermore, the porous structure could help the target gas pass through the sensing layer quickly, thereby reducing gas consumption.

The gas sensing performance for a sensor based on YSZ solid electrolyte and metal oxide SE is closely related to its operating temperature. The response change of gas sensor toward 100 ppm C_2H_2 at 650 °C, 675 °C, 700 °C, 725 °C, and 750 °C is shown in Fig. 3(a). Before 700 °C, the response value of the gas sensor based on porous SnO_2/Zn_2SnO_4-SE gradually improved as the operating temperature increased. However, the response value decreased when the working temperature was more than 700 °C. Therefore, 700 °C could be deemed as the most appropriate operating temperature for the present sensor, and the following sensing measurement was conducted at such an operating temperature. Fig. 3(b) depicts the response transients of the sensor toward C_2H_2 in the concentration range from 0.5 ppm to 1000 ppm at 700 °C. The developed sensing device that used porous SnO_2/Zn_2SnO_4-SE showed good response and recovery characteristics to 0.5–1000 ppm C_2H_2. In addition, the response signal gradually improved when the C_2H_2 concentration increased. The response value of the sensor to 100 ppm C_2H_2 was −82.3 mV, and the detection limit of C_2H_2 was 0.5 ppm; its response value was −2.1 mV at 700 °C. The time of response and recovery is one of the most important parameters of the gas sensor in practical applications. The response time for the porous SnO_2/Zn_2SnO_4-SE sensor refers to the time arriving at 90% of the stable electric potential value when the sensor was placed in the sample gas.

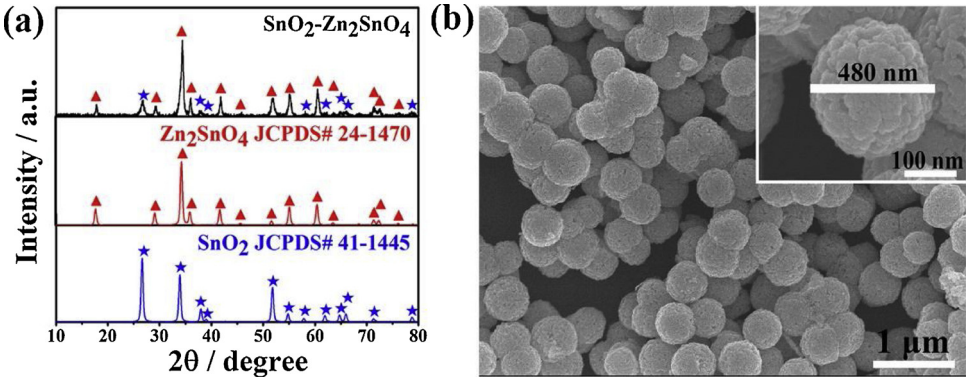

Fig. 2. XRD pattern (a) and SEM image (b) of SnO_2/Zn_2SnO_4 sensing material sintered at 800 °C.

By contrast, the recovery time is the time when the sensor was removed from the sample gas, reaching 90% of the stable electric potential value in air. As shown in Fig. 3(c), the response and recovery times were 7 and 15 s toward 100 ppm C_2H_2 at 700 °C, respectively. This result demonstrated that the sensor with SnO_2/Zn_2SnO_4-SE possessed rapid response speed and quick recovery capacity. Fig. 3(d) shows the piecewise negative linear relationship between the electric potential difference and the logarithm of the C_2H_2 concentrations in the ranges of 0.5–2 ppm and 5–1000 ppm, with sensitivities of −12 and −56 mV / decade, respectively. The reason for this linear relationship phenomenon could be explained by the mixed-potential sensing mechanism. According to previous studies [35–40], on the TPB of C_2H_2/YSZ/SnO_2/Zn_2SnO_4-SE, the electrochemical cathodic reaction of O_2 and the electrochemical anodic reaction of C_2H_2 occur simultaneously and form a local cell at the SE to determine the mixed potential to C_2H_2. When the rates of two electrochemical reactions reach a dynamic equilibrium, the electrode potential is called the mixed potential. The potential difference of the SE and the RE is obtained as the sensing response signal.

$$\text{Anodic reaction: } C_2H_2 + 5O^{2-} \rightarrow 2CO_2 + H_2O + 10e^- \quad (1)$$

$$\text{Cathodic reaction: } 5/2O_2 + 10e^- \rightarrow 5O^{2-} \quad (2)$$

The electric potential response of the mixed-potential-type sensor can be illuminated following the Butler–Volmer equation. Primarily, the current density equations of reactions (1) and (2) are listed as (3) and (4):

$$i_{C_2H_2} = i^0_{C_2H_2} \exp[2\alpha_1 F(V - V^0_{C_2H_2})/RT] \quad (3)$$

$$i_{O_2} = i^0_{O_2} \exp[-2\alpha_2 F(V - V^0_{O_2})/RT] \quad (4)$$

Therein, i^0, α, F, V, and V^0 represent the exchange current density, transfer coefficient, Faraday constant, electrode potential, and equilibrium electrode potential, respectively; R denotes the gas constant, and T is temperature. The exchange current density is accorded with the kinetic Eq. (5) and (6):

$$i^0_{C_2H_2} = B_1 C^n_{C_2H_2} \quad (5)$$

$$i^0_{O_2} = -B_2 C^m_{O_2} \quad (6)$$

$C_{C_2H_2}$ and C_{O_2}represent the concentration in C_2H_2 and O_2; B_1, B_2, m and n are constant. When the rates of reactions (1) and (2) achieve dynamic equilibrium, $i_{C_2H_2} = -i_{O_2}$ or $|i_{C_2H_2}| = |-i_{O_2}|$, the potential (V) is named as the mixed potential (V_M).

$$V_M = V_0 + mA \ln C_{O_2} - nA \ln C_{C_2H_2} \quad (7)$$

Above equation,

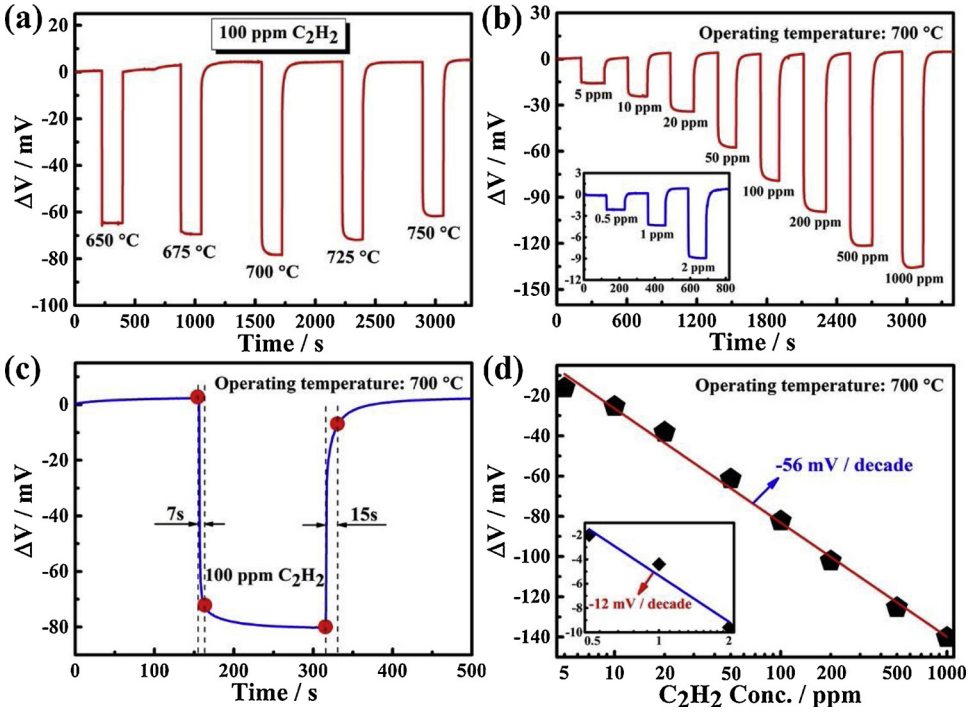

Fig. 3. (a) Effect of the operating temperature on C_2H_2 sensing performance of the sensor using porous SnO_2/Zn_2SnO_4-SE; (b) Response transients for the sensor toward 0.5–1000 ppm C_2H_2 at 700 °C; (c) Response and recovery characteristics of the sensor to 100 ppm C_2H_2; (d) Dependence of ΔV for the sensor on the logarithm of C_2H_2 concentrations at 700 °C.

$$V_0 = \frac{RT}{(2\alpha_1 + 2\alpha_2)F}\ln\frac{B_2}{B_1} + \frac{\alpha_1 V^0_{C_2H_2} + \alpha_2 V^0_{O_2}}{\alpha_1 + \alpha_2} \quad (8)$$

$$A = \frac{RT}{(2\alpha_1 + 2\alpha_2)F} \quad (9)$$

If the O_2 concentration was a fixed value, Eq. (7) becomes

$$V_M = V_0 - nA\ln C_{C_2H_2} \quad (10)$$

From Eq. (10), the potential response value of the sensor varied linearly negatively to the C_2H_2 concentration in the case of fixed O_2 concentration, which is in accordance with the results in Fig. 3(d). However, the sensitivity of the sensor to C_2H_2 in the range of 5–1000 ppm was much higher than the concentration range of 0.5–2 ppm C_2H_2, which may be explained by the diffusion consumption process of C_2H_2 in the porous SnO_2/Zn_2SnO_4 SE layer. As shown in Fig. 2(b), the SnO_2 /Zn_2SnO_4 with porous structure contributed to the diffusion of large quantities of C_2H_2 in the SE, and more C_2H_2 gas arrived at TPB. However, according to previous studies [23,45,46], the C_2H_2 gas must move through the SE diffusion layer prior to reaching the TPB due to the catalytic characteristics of SE at 700 °C. Then, C_2H_2 will react with oxygen by the gas phase catalytic reaction: $C_2H_2 + 5/2\ O_2 \rightarrow 2CO_2 + H_2O$ to produce carbon dioxide, thereby resulting in a certain amount of gas being consumed. At a low C_2H_2 concentration range (0.5–2 ppm), the amount of TPB active sites is sufficient to produce an electrochemical reaction; thus, the sensitivity of the sensor is mainly attributed to the amount of C_2H_2 reaching the TPB. The C_2H_2 consumption proportion that accounted for the total quantity of C_2H_2 in the diffusion process is larger than the concentration range of C_2H_2 (5–1000 ppm). As a result, less C_2H_2 participated in the electrochemical reaction at TPB. Therefore, the sensitivity of −12 mV / decade to 0.5–2 ppm C_2H_2 was lower compared with that of 5–1000 ppm C_2H_2.

The oxygen concentration is also an important effect parameter of the sensing characteristics of a developed gas sensor. Fig. 4 shows the dependence of the potential response variation to 50 ppm C_2H_2 on O_2 in the concentration range of 2%–21% at 700 °C. The response value of the sensor to 50 ppm C_2H_2 at 700 °C increased with the decrease of O_2 concentration, and the degree of change was acceptable (Fig. 4(a)). Moreover, at 700 °C, the potential value of the sensor to C_2H_2 and the logarithm of O_2 concentration exhibited a positive linear variation, which had been confirmed in Eq. (7). Continuous response–recovery curves to 100 ppm C_2H_2 for the sensor based on porous SnO_2/Zn_2SnO_4-SE at 700 °C are shown in Fig. 5. After 10 cycles, the response and recovery transients could repeat perfectly, thereby indicating that the prepared device revealed good reproducibility to 100 ppm C_2H_2 at 700 °C.

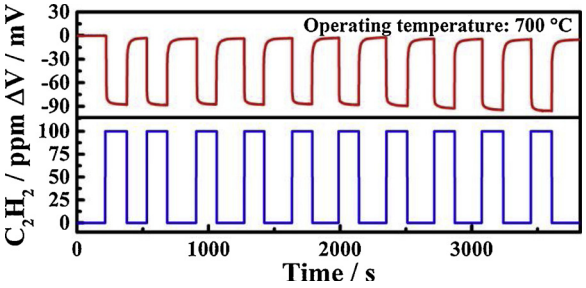

Fig. 5. Continuous response-recovery curves to 100 ppm C_2H_2 for the sensor based on porous SnO_2/Zn_2SnO_4-SE at 700 °C.

Gas sensors often work in environments with high water vapor content; thus, their humidity resistance was also widely concerned. As shown in Fig. 6(a), the response and recovery curves of the gas sensor with porous SnO_2/Zn_2SnO_4-SE toward 50 ppm C_2H_2 in 20% RH, 40% RH, 60% RH, 80% RH, and 98% RH showed a nearly uniform trend. In Fig. 6(b), the response value of the gas sensor to 50 ppm C_2H_2 in different relative humidity exhibited slight fluctuation, thereby indicating that the prepared sensing device can maintain stable C_2H_2 sensing characteristics in a high-humidity environment.

The cross-sensitivities to various gases were measured and appraised for the fabricated device based on porous SnO_2/Zn_2SnO_4-SE at 700 °C. As seen in Fig. 7(a), the potential difference to 100 ppm C_2H_2 at

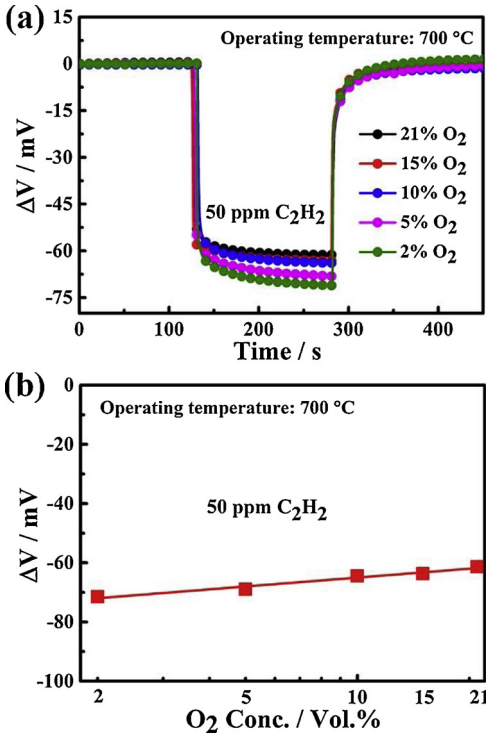

Fig. 4. (a) Response and recovery curves of the sensor attached with porous SnO_2/Zn_2SnO_4-SE to 50 ppm C_2H_2 under 2%–21% O_2 at 700 °C; (b) Dependence of ΔV on the logarithm of O_2 concentrations.

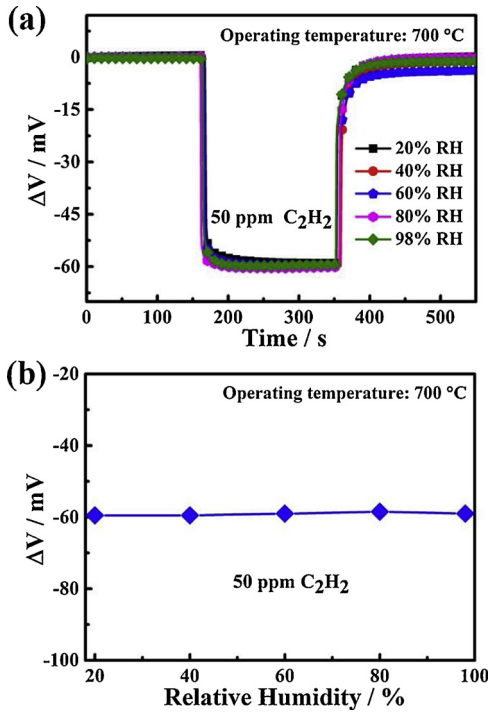

Fig. 6. (a) Response and recovery curves of the sensor to 50 ppm C_2H_2 at 20%–98% relative humidity; (b) Variation of response value for the sensor to 50 ppm C_2H_2 at different relative humidity.

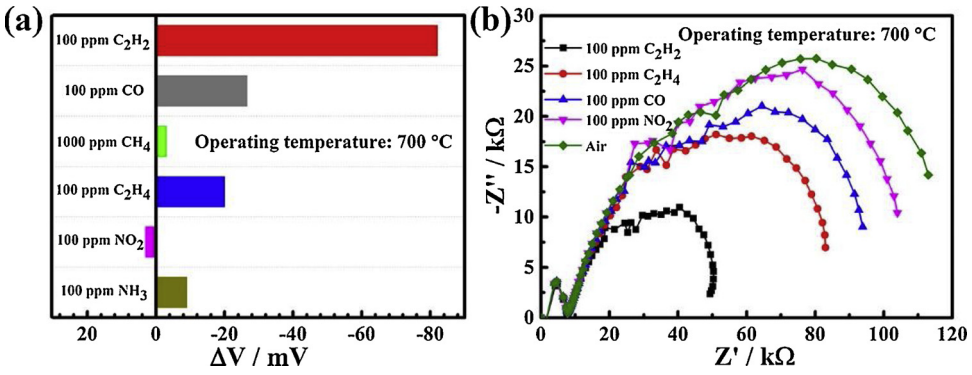

Fig. 7. (a) Selectivity and (b) complex impedance curves of the fabricated sensor to various gases at 700 °C.

700 °C achieved the highest value compared with the potential response value of other gases. This result demonstrated that the sensor using porous SnO_2/Zn_2SnO_4-SE displayed good selectivity to C_2H_2 at 700 °C. Furthermore, the complex impedance curves in different gases were investigated to account for the reason why the sensor with porous SnO_2/Zn_2SnO_4 showed good selectivity to C_2H_2. The relevant results are shown in Fig. 7(b). As reported in the literature [41–44], the resistance of the sensor at high frequencies is mainly attributed to SE bulk resistance (including the small YSZ-bulk resistance). However, the interfacial resistance between the YSZ substrate and the sensing material is the main factor that affects the total resistance of the device, and it is given by the resistance value at the intersection of the large semi-arc with the real axis at low frequencies (approximately 0.1 Hz). At different interface resistances measured in different gases, SnO_2/Zn_2SnO_4-SE displayed various electrochemical catalytic activity toward the examined gas species. Fig. 7(b) shows that the resistance at high frequencies was almost invariable when exposed at different tested gas atmosphere. By contrast, the distinct resistance value difference for the sensor to different test gases in the low-frequency range was observed, and the interfacial resistance in 100 ppm C_2H_2 was the smallest compared with 100 ppm CO, CH_4, C_2H_4, NO_2, and NH_3. Thus, we deduced that the catalytic activity of the SnO_2/Zn_2SnO_4-SE to the electrochemical reaction of C_2H_2 was the largest, which generated the highest response toward C_2H_2. To verify the mixed-potential theory of the prepared sensor, the polarization curves were measured in air and different concentrations of C_2H_2 at 700 °C. As shown in Fig. 8, the cathodic polarization curve was gained in air, and the anodic polarization curve was acquired by subtracting the current value in air from the current value in different concentrations of C_2H_2. The intersection (estimated value) of the anodic and cathodic polarization curve is defined as the mixed potential. Evidently, the estimated values (−78 and −87 mV) in 100 and 200 ppm C_2H_2 were almost similar to the observed values (−81.5 and −90.5 mV) on the basis of the experimental measurement.

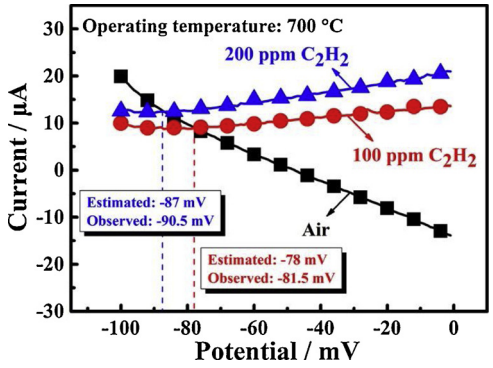

Fig. 8. Polarization curves in different concentrations of C_2H_2 for the sensor utilizing porous SnO_2/Zn_2SnO_4-SE.

The long-term stability of the prepared sensor was assessed by measuring the response value change to 100 ppm C_2H_2 at 700 °C for 20 consecutive days. Fig. 9(a) shows that the response value was almost maintained at −80 mV, and an attenuation percentage less than 9% is acceptable. Furthermore, Fig. 9(b) shows the relatively good response and recovery curves of the prepared sensor to 100 ppm C_2H_2 in the original and at 6th, 12th, 18th, and 20th days. Furthermore, the sensing performance of the manufactured sensor with porous SnO_2/Zn_2SnO_4 SE sintered at 800 °C after 20 days was tested. The continuous response and recovery curves for the developed device to C_2H_2 in the range of 0.5–1000 ppm at 700 °C are shown in Fig. 9(c). The present sensing device exhibited good response and recovery characteristics to different concentrations of C_2H_2 at 700 °C. Simultaneously, the sensitivity of the sensor to 0.5–1000 ppm C_2H_2 exhibited a negative linear relationship, wherein the slope of 5–1000 ppm C_2H_2 concentration was -49 and −14 mV/ decade in the range of 0.5–2 ppm C_2H_2. The sensor still achieved the lowest detection limit of 0.5 ppm to C_2H_2 after 20-day measurement. Compared with the sensitivity before 20 days, a slight change was observed in the lower concentration range (0.5–2 ppm) and higher concentration range (5–1000 ppm) to C_2H_2 after 20 days of high-temperature measurement. As shown in Fig. 9(e), the prepared sensor could still perform the successive reduplicative potential response to 100 ppm C_2H_2 at 700 °C after 20 days, demonstrating that the sensor attached with SnO_2/Zn_2SnO_4-SE had comparatively excellent reproducibility and stability. All the above experimental results indicated that the sensor we prepared can present good stability after a long operation time at high temperature. Therefore, the YSZ solid electrolyte-type sensor combined with porous SnO_2/Zn_2SnO_4-SE has potential application value in detecting C_2H_2.

4. Conclusion

In conclusion, this study is the first to establish a YSZ-based mixed-potential-type C_2H_2 sensor with porous SnO_2/Zn_2SnO_4 composite oxide SE. The porous SnO_2/Zn_2SnO_4 sensing material was synthesized by a facile hydrothermal method. The material had a spherical diameter of 480 nm and a porous structure. The constructed sensor using porous SnO_2/Zn_2SnO_4 exhibited fast response and recovery characteristics and good stability and reproducibility before and after 20 days of high-temperature measurement. After 20 days of high-temperature measurement, the response value of the device to 100 ppm C_2H_2 displayed a change amplitude of −0.97% at 700 °C. The lowest detection limit of the sensing device to C_2H_2 was 0.5 ppm, and the changes of sensitivity in the C_2H_2 concentration range of 0.5–2 and 5–1000 ppm were −14 and −49 mV/decade, respectively. The mixed-potential gas sensor based on YSZ and porous SnO_2/Zn_2SnO_4-SE can be used to detect C_2H_2.

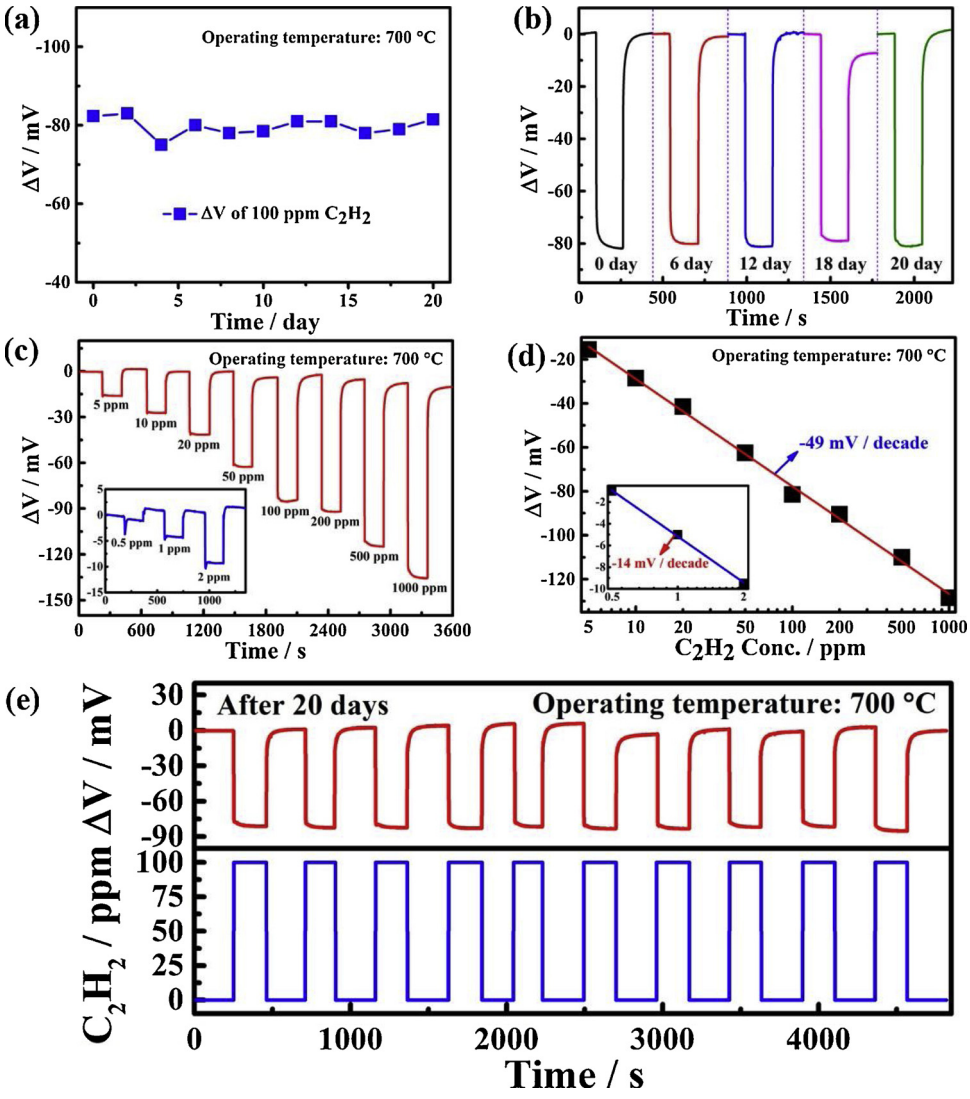

Fig. 9. (a, b) Long-term stability of the sensor working at 700 °C in the presence of 100 ppm C_2H_2; (c, d) Response transients and sensitivity for the sensor toward 0.5–1000 ppm C_2H_2 at 700 °C after 20 days high temperature stability; (e) the continuous response-recovery curves to 100 ppm C_2H_2 for the sensor after 20 days measurement at 700 °C.

Acknowlegements

This work is supported by the National Nature Science Foundation of China (Nos. 61831011, 61327804, 61520106003 and 61803171), Program for Chang Jiang Scholars and Innovative Research Team in University (No. IRT13018), National Key Research and Development Program of China (Nos. 2016YFC0207300 and 2016YFC 0201002), Application and Basic Research of Jilin Province (20130102010 JC), Young Elite Scientists Sponsorship Program by CAST (2018QNRC001), Program for JLU Science and Technology Innovative Research Team (JLUSTIRT 2017TD-07), The Fundamental Research Funds for the Central Universities, China Postdoctoral Science Foundation funded project (No. 2018M630322).

References

[1] A. Akbari, A. Setayeshmehr, H. Borsi, E. Gockenbach, I. Fofana, Intelligent agent-based system using dissolved gas analysis to detect incipient faults in power transformers, IEEE Electr. Insul. Mag. 26 (2010) 27–40.
[2] V.G. Arakelian, The long way to the automatic chromatographic analysis of gases dissolved in insulating oil, IEEE Electr. Insul. Mag. 20 (2004) 8–25.
[3] M. Duval, J. Dukarm, Improving the reliability of transformer gas-in-oil diagnosis, IEEE electr. Insul. Mag. 21 (2005) 21–27.
[4] A.S.M.I. Uddin, D.T. Phan, G.S. Chung, Low temperature acetylene gas sensor based on Ag nanoparticles-loaded ZnO-reduced graphene oxide hybrid, Sens. Actuators B: Chem. 207 (2015) 362–369.
[5] C.S. Lee, J.H. Choi, Y.H. Park, Development of metal-loaded mixed metal oxides gas sensors for the detection of lethal gases, J. Ind. Eng. Chem. 29 (2015) 321–329.
[6] A. Mirzaei, S.G. Leonardi, G. Neri, Detection of hazardous volatile organic compounds (VOCs) by metal oxide nanostructures-based gas sensors: a review, Ceram. Int. 42 (2016) 15119–15141.
[7] N. Maksymovych, O. Ripko, O. Maksymovych, O. Kaskevych, N. Nikitina, V. Ruchko, O. Kuzko, V. Yatsimirsky, Adsorption semiconductor detector for malfunction diagnosis of high voltage transformers, Sens. Actuators B: Chem. 93 (2003) 321–326.
[8] Z. Wu, Y. Gong, Q. Yu, Photoacoustic spectroscopy detection and extraction of discharge feature gases in transformer oil based on 1.5 mu tunable fiber laser, Infrared Phys. Technol. 58 (2013) 86–90.
[9] X. Li, Y. Xia, J. Huang, L. Zhan, A Raman system for multi-gas-species analysis in power transformer, Appl. Phys. B-Lasers Opt. 93 (2008) 665–669.
[10] W. Chen, B. Liu, H. Huang, Photoacoustic sensor signal transmission line model for gas detection in transformer oil, Sens Lett. 9 (2011) 1511–1514.
[11] N. Tamaekong, C. Liewhiran, A. Wisitsoraat, S. Phanichphant, Acetylene sensor based on Pt/ZnO thick films as prepared by flame spray pyrolysis, Sens. Actuators B: Chem. 152 (2011) 155–161.
[12] F. Liu, Y. Wang, B. Wang, X. Yang, Q. Wang, X. Liang, P. Sun, X. Chuai, Y. Wang, G. Lu, Stabilized zirconia-based mixed potential type sensors utilizing $MnNb_2O_6$ sensing electrode for detection of low-concentration SO_2, Sens. Actuators B: Chem. 238 (2017) 1024–1031.
[13] A.S.M. Iftekhar uddin, K.-W. Lee, G.-S. Chung, Acetylene gas sensing properties of an Ag-loaded hierarchical ZnO nanostructure-decorated reduced graphene oxide hybrid, Sens. Actuators B: Chem. 216 (2015) 33–40.
[14] C. Liewhiran, N. Tamaekong, A. Wisitsoraat, S. Phanichphant, Highly selective

environmental sensors based on flame-spray-made SnO_2 nanoparticles, Sens. Actuators B: Chem. 163 (2012) 51–60.
[15] A.S.M. Iftekhar Uddin, G.-S. Chung, Effects of Ag nanoparticles decorated on ZnO nanorods under visible light illumination on flexible acetylene gas sensing properties, J. Electroceram. 40 (2018) 42–49.
[16] A.S.M. Iftekhar Uddin, D.-T. Phan, G.-S. Chung, Low temperature acetylene gas sensor based on Ag nanoparticles-loaded ZnO-reduced graphene oxide hybrid, Sens. Actuators B: Chem. 207 (2015) 362–369.
[17] N. Miura, J. Wang, M. Nakatou, P. Elumalai, S. Zhuiykov, M. Hasei, High-temperature operating characteristics of mixed-potential-type NO_2 sensor based on stabilized-zirconia tube and NiO sensing electrode, Sens. Actuators B: Chem. 114 (2006) 903–909.
[18] F. Liu, Y. Guan, H. Sun, X. Xu, R. Sun, X. Liang, P. Sun, Y. Gao, G. Lu, YSZ-based NO_2 sensor utilizing hierarchical In_2O_3 electrode, Sens. Actuators B: Chem. 222 (2016) 698–706.
[19] P.K. Sekhar, R. Mukundan, E. Brosha, F. Garzon, Effect of perovskite electrode composition on mixed potential sensor response, Sens. Actuators B: Chem. 183 (2013) 20–24.
[20] H.T. Giang, H.T. Duy, P.Q. Ngan, G.H. Thai, D.T.A. Thu, D.T. Thu, N.N. Toan, High sensitivity and selectivity of mixed potential sensor based on Pt/YSZ/$SmFeO_3$ to NO_2 gas, Sens. Actuators B: Chem. 183 (2013) 550–555.
[21] G. Lu, N. Miura, N. Yamazoe, High-temperature sensors for NO and NO_2 based on stabilized zirconiaand spinel-type oxide electrodes, J. Mater. Chem. 7 (1997) 1445–1449.
[22] Y. Guan, C. Yin, X. Cheng, X. Liang, Q. Diao, H. Zhang, G. Lu, Sub-ppm H_2S sensor based on YSZ and hollow balls $NiMn_2O_4$ sensing electrode, Sens. Actuators B: Chem. 193 (2014) 501–508.
[23] F. Liu, R. Sun, Y. Guan, X. Cheng, H. Zhang, Y. Guan, X. Liang, P. Sun, G. Lu, Mixed-potential type NH_3 sensor based on stabilized zirconia and $Ni_3V_2O_8$ sensing electrode, Sens. Actuators B: Chem. 210 (2015) 795–802.
[24] F. Liu, Y. Guan, X. Liang, R. Sun, X. Liang, P. Sun, F. Liu, G. Lu, Mixed potential type acetone sensor using stabilized zirconia and $M_3V_2O_8$ (M: Zn, Co and Ni) sensing electrode, Sens. Actuators B: Chem. 221 (2015) 673–680.
[25] M. Batzill, U. Diebold, The surface and materials science of tin oxide, Prog. Surf. Sci. 79 (2005) 47–154.
[26] O. Lupan, L. Chow, G. Chai, H. Heinrich, S. Park, A. Schulte, Growth of tetragonal SnO_2 microcubes and their characterization, J. Cryst. Growth. 311 (2008) 152–155.
[27] H. Khallaf, C.T. Chen, L.B. Chang, O. Lupan, A. Dutta, H. Heinrich, F. Haque, E.D. Barco, L. Chow, Chemical bath deposition of SnO_2 and Cd_2SnO_4 thin films, Appl. Surf. Sci. 258 (2012) 6069–6074.
[28] T.J. Coutts, D.L. Young, X. Li, W.P. Mulligan, X. Wu, Search for improved transparent conducting oxides: a fundamental investigation of CdO, Cd_2SnO_4, and Zn_2SnO_4, J. Vac. Sci. Technol. A. 18 (2000) 2646–2660.
[29] Z. Chen, M. Cao, C. Hu, Novel Zn_2SnO_4 hierarchical nanostructures and their gas sensing properties toward ethanol, J. Phys. Chem. C. 115 (2011) 5522–5529.
[30] C. Pang, B. Yan, L. Liao, B. Liu, Z. Zheng, T. Wu, H. Sun, T. Yu, Synthesis, characterization and opto-electrical properties of ternary Zn_2SnO_4 nanowires, Nanotechnology 21 (2010) 465706.
[31] J.H. Yu, G.M. Choi, Selective CO gas detection of Zn_2SnO_4 gas sensor, J. Electroceram. 8 (2002) 249–255.
[32] Y. Jiang, C. He, R. Sun, Z. Xie, L. Zheng, Synthesis of Zn_2SnO_4 nanoplate-built hierarchical cube-like structures with enhanced gas-sensing property, Mater. Chem. Phys. 136 (2012) 698–704.
[33] G. Lu, Q. Diao, C. Yin, S. Yang, Y. Guan, X. Cheng, X. Liang, High performance mixed-potential type NO_x sensor based on stabilized zirconia and oxide electrode, Solid State Ion 262 (2014) 292–297.
[34] X. Yang, Q. Yu, S. Zhang, P. Sun, H. Lu, X. Yan, F. Liu, X. Zhou, X. Liang, Y. Gao, G. Lu, Highly sensitive and selective triethylamine gas sensor based on porous SnO_2/Zn_2SnO_4 composites, Sens. Actuators B: Chem. 266 (2018) 213–220.
[35] N. Miura, G. Lu, M. Ono, N. Yamazoe, Selective detection of NO by using an amperometric sensor based on stabilized zirconia and oxide electrode, Solid State Ionics 117 (1999) 283–290.
[36] F. Garzon, R. Mukundan, E. Brosha, Solid-state mixed potential gas sensors: theory, experiments and challenges, Solid State Ionics 136–137 (2000) 633–638.
[37] G. Lu, N. Miura, N. Yamazoe, Stabilized zirconia-based sensors using WO_3 electrode for detection of NO or NO_2, Sens. Actuators B: Chem. 65 (2000) 125–127.
[38] Y. Liu, J. Parisi, X. Sun, Y. Lei, Solid-state gas sensors for high temperature applications – a review, J. Mater. Chem. A 2 (2014) 9919–9943.
[39] N. Miura, T. Sato, S.A. Anggraini, H. Ikeda, S. Zhuiykov, A review of mixed-potential type zirconia-based gas sensors, Ionics 20 (2014) 901–925.
[40] C.O. Park, J.W. Fergus, N. Miura, J. Park, A. Choi, Solid-state electrochemical gas sensors, Ionics 15 (2009) 261–284.
[41] F. Liu, X. Yang, B. Wang, Y. Guan, X. Liang, P. Sun, G. Lu, High performance mixed potential type acetone sensor based on stabilized zirconia and $NiNb_2O_6$ sensing electrode, Sens. Actuators B: Chem. 229 (2016) 200–208.
[42] N. Miura, M. Nakatou, S. Zhuiykov, Impedance-based total-NO_x sensor using stabilized zirconia and $ZnCr_2O_4$ sensing electrode operating at high temperature, Electrochem. Commun. 4 (2002) 284–287.
[43] M. Stranzenbach, E. Gramckow, B. Saruhan, Planar, impedance-metric NOx -sensor with spinel-type SE for high temperature applications, Sens. Actuators B: Chem. 127 (2007) 224–230.
[44] H. Jin, Y. Huang, J. Jian, Sensing mechanism of the zirconia-based highly selective NO sensor by using a plate-like Cr_2O_3 sensing electrode, Sens. Actuators B: Chem. 219 (2015) 112–118.
[45] J.W. Fergus, Sensing mechanism of non-equilibrium solid-electrolyte-based chemical sensors, J. Solid State Electrochem. 15 (2011) 971–984.
[46] S.A. Anggraini, Y. Fujio, H. Ikeda, N. Miura, YSZ-based sensor using Cr-Fe-based spinel-oxide electrodes for selective detection of CO, Anal. Chim. Acta 982 (2017) 176–184.